Carrier dynamics in bulk ZnO. I. Intrinsic conductivity measured by terahertz time-domain spectroscopy

Jason B. Baxter[1,*,†] and Charles A. Schmuttenmaer[2,*,‡]
[1]*Department of Chemical and Biological Engineering, Drexel University, 3141 Chestnut Street, Philadelphia, Pennsylvania 19083, USA*
[2]*Chemistry Department, Yale University, P.O. Box 208107, 225 Prospect Street, New Haven, Connecticut 06520, USA*
(Received 12 August 2009; published 30 December 2009)

Far-infrared absorption and refractive index of a ZnO wafer were measured as a function of temperature below 120 K using terahertz (THz) time domain spectroscopy. The accompanying frequency-dependent complex conductivity gives an accurate picture of electron dynamics because the measured range of 0.2–2.5 THz brackets the scattering rate. The frequency-dependent conductivity shows the general trends predicted by the Drude model but with significant deviations that are better fit by the generalized Drude model, which allows for a distribution of carrier relaxation times. Conductivity increases with increasing temperature as electrons are thermally activated from shallow donor states, with calculated donor energy of 27 meV and density of 1.4×10^{17} cm^{-3}. Mobilities of ~2000 cm^2 V^{-1} s^{-1} are measured and do not vary significantly with temperature over 60–120 K.

DOI: 10.1103/PhysRevB.80.235205 PACS number(s): 72.20.−i, 72.80.Ey, 78.20.Ci, 71.55.Gs

I. INTRODUCTION

ZnO is a wide band-gap semiconductor (E_g=3.37 eV at 4 K) with 60 meV exciton binding energy that has received much recent attention for optoelectronic applications.[1,2] ZnO is a very strong emitter of near-UV light, and lasing has been demonstrated at room temperature.[3] Thin films of ZnO are useful in transparent transistors and transparent conducting coatings because of their combination of wide band gap, high conductivity, and processability.[4,5] Additionally, ZnO wafers are frequently used as substrates for epitaxial GaN growth because they possess the same wurtzite structure and similar lattice parameters, and bulk crystal growth is significantly easier for ZnO than GaN.[6] Bulk ZnO crystals have been grown hydrothermally,[7] by vapor phase transport,[8] and from the melt.[9]

ZnO is intrinsically *n* type due to native defects such as Zn interstitials, Zn_I, and O vacancies, V_O.[1] Additionally, density functional theory[10] and infrared spectroscopy[11–13] have shown that hydrogen also acts as a shallow donor. The difficulty in avoiding these defects, particularly hydrogen, has made growing *p*-type ZnO challenging,[14] although significant progress has recently been made in this area.[15,16] Room-temperature electron mobilities of ~200 cm^2 V^{-1} s^{-1} have been reported by multiple groups using Hall-effect measurements.[7–9,17] We recently reported similar room-temperature mobilities, which we determined using terahertz time-domain spectroscopy (THz-TDS).[18] THz-TDS indicated mobilities of 232 cm^2 V^{-1} s^{-1} for thin films, 189 cm^2 V^{-1} s^{-1} for nanowires, and 110 cm^2 V^{-1} s^{-1} for mesoporous nanoparticle films, where increasing amounts of surface and interface scattering reduced the mobility in the smaller grained nanostructures. Several bulk scattering mechanisms can also be active in ZnO depending on temperature and material purity, including ionized impurity scattering, optical and acoustic phonon scattering, piezoelectric scattering, and scattering from native defects and dislocations.[1] Using temperature-dependent Hall measurements, Look *et al.* determined the donor energies to be 31 and 61 meV in a wafer grown by vapor phase transport.[17] The smaller of these barriers was assigned to Zn_I, while the larger was believed to be hydrogenic. Additionally, Hall measurements showed mobilities increasing from ~200 cm^2 V^{-1} s^{-1} at room temperature to a maximum of 1900 cm^2 V^{-1} s^{-1} at 60 K before decreasing to below 300 cm^2 V^{-1} s^{-1} at 15 K.[8] The temperature dependence of their mobility data was well-fit by using Rode's method to solve the Boltzmann transport equation.[19]

While Hall measurements can provide reliable measurements over a wide range of conductivity, they measure only dc or low-frequency conductivities, can be distorted by surface defects, and require making contacts to the wafer. Alternatively, THz-TDS measures the frequency-dependent complex conductivity in the far-infrared region using a noncontact optical probe in transmission geometry.[20] Coherent detection of a single-cycle THz pulse in the time domain allows the amplitude and phase to be determined independently in the frequency domain. Absorbance and refractive index, and consequently real and imaginary conductivity, can be determined over the range of 0.2–2.5 THz without the need for Kramers-Kronig analysis. Conductivity models, such as that proposed by Drude, can then be fit to the data to extract carrier densities and mobilities. THz-TDS has been employed to measure conductivity in a host of materials including bulk Si,[21,22] polymers,[23,24] doped ZnO thin films,[25] and nanostructured intrinsic ZnO.[18]

In this paper, we report the temperature-dependent conductivity of a ZnO wafer measured by THz-TDS. Conductivity is derived from permittivity measurements using the permittivity at 10 K as a reference. We find that the Drude model can describe conductivity behavior to first order but that significant systematic deviations from the model exist. The generalized Drude (GD) model, which includes a distribution of relaxation times, fits the experimental data much more accurately. Carrier densities extracted from these models increase exponentially in the temperature range of 40–120 K due to thermal activation from donor states, with an activation energy of 27 meV. Mobilities of

$\sim$2000 $cm^2\ V^{-1}\ s^{-1}$ were found in this temperature range, independent of temperature.

II. EXPERIMENTAL METHODS

The ZnO wafer studied was grown from the melt by Cermet, Inc. and is nominally undoped but displays *n*-type conductivity. The wafer is 10×10 mm, 380 μm thick, and (0001) cut. It was mounted to cover a 6 mm aperture in a brass holder with neighboring 6 mm aperture open to allow for reference measurements. The holder was mounted in a helium-cooled optical cryostat (Janis model ST-100, with LakeShore model 321 temperature controller) to allow measurements to below 10 K.

An amplified Ti:Sapphire laser (Tsunami/Spitfire from Spectra Physics) was used to generate 800 mW of pulsed near-IR light at 1 kHz. The pulse width was $\sim$100 fs, and the center wavelength was 800 nm. The near-IR light was used to generate THz radiation using optical rectification in a ZnTe(110) crystal. A series of four parabolic mirrors focuses the THz radiation to a spot size of $\sim$3 mm at the sample and then onto a second ZnTe(110) crystal for detection by free space electro-optic sampling. The THz beam path was purged with dry nitrogen, although some spurious water absorption still remains at around 1.6 THz due to slight differences in humidity between scans. Details on the THz spectrometer have been published previously.[26]

The frequency-dependent complex permittivity of the ZnO was determined by THz-TDS. Terahertz wave forms were recorded in the time domain with and without the ZnO wafer in the beam path, where the latter is simply the reference pulse. The power, P, and phase, ϕ, were calculated by Fourier transform of the time domain scans, and the absorption coefficient and refractive index were determined using

$$\alpha = -\frac{1}{d}\ln\left(\frac{P}{P_0}\right) \tag{1}$$

and

$$n = 1 + \frac{c}{2\pi\omega d}(\phi - \phi_0), \tag{2}$$

where P_0 and ϕ_0 are the power and phase at a given frequency ω for the reference pulse and P and ϕ are for the pulse that has passed through the sample. The wafer thickness is d, and c is the speed of light. Time-domain spectra were truncated before the first ZnO internal reflection to eliminate etaloning effects.

III. RESULTS AND DISCUSSION

The frequency-dependent absorption coefficient and refractive index of the ZnO wafer were measured as a function of temperature from 10 to 120 K and are shown in Fig. 1. At low frequencies ($\leq$0.5 THz), the absorption coefficient increases from nearly zero to almost 400 cm^{-1} with increasing temperature due to free-carrier absorption by electrons that are thermally excited into the conduction band from shallow donor states [Fig. 1(a)]. As a result of the increased carrier

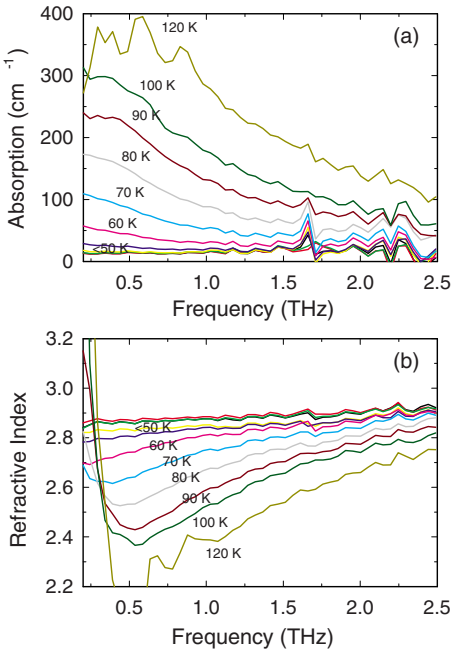

FIG. 1. (Color online) (a) Absorption and (b) refractive index of a ZnO wafer in the THz frequency range for temperatures ranging from 10 to 120 K. Increased absorption and decreased refractive index at higher temperatures results from higher densities of electrons that have been thermally excited into the conduction band.

concentration, the absorption peak also shifts to higher frequency with increasing temperature, from less than 0.2 THz below 80 K to 0.6 THz at 120 K. At low temperature, ZnO absorption is extremely small, with the 15 cm^{-1} offset in the absorption spectra due to reflection losses. Reliable measurements could not be made above 120 K or below 0.2 THz because the sample absorption exceeded the dynamic range of the spectrometer in those regions.[27] Above 120 K, absorption by thermally generated free carriers reduced THz transmission to less than 0.5%.

The refractive index also depends strongly on temperature due to the increasing number of carriers, as seen in Fig. 1(b). At 10 K, the refractive index is 2.9 and is nearly independent of frequency. At higher temperatures, the refractive index approaches 2.9 at high frequencies, exhibits a minimum at or below 0.5 THz, and increases rapidly as the frequency approaches dc. The low-temperature frequency-dependent absorption coefficient and refractive index agree well with room-temperature measurements of a highly insulating ZnO wafer by Azad *et al.*,[28] who reported absorption less than 25 cm^{-1} and refractive index of 2.8, both of which rise slightly with increasing frequency due to a phonon mode at 12.4 THz. Additionally, the trends in absorbance and refractive index with increasing carrier concentrations that result from increased thermal energy are similar to those reported by van Exter and Grischkowsky for different Si wafers of increasing doping densities measured at room temperature and 80 K.[22] The frequency dependence of the absorption coefficient and refractive index as a function of carrier density shows classic Drude-like behavior.

The frequency-dependent, complex-valued conductivity, $\hat{\sigma}$, arising from thermally-excited conduction-band electrons is obtained from

$$\hat{\eta}(\omega) = \hat{\varepsilon}(\omega) + \frac{i\hat{\sigma}(\omega)}{\varepsilon_0 \omega}, \tag{3}$$

where $\hat{\eta}$ is the generalized permittivity, $\hat{\varepsilon}$ is the permittivity due to bound charges, ω is the angular frequency, ε_0 is the free-space permittivity, and i is the unit imaginary. The complex-valued permittivity and the complex-valued refractive index are related through $\hat{\varepsilon}=\hat{n}^2$, where $\hat{n}=n+ik$, and $k=\lambda\alpha/4\pi=c\alpha/2\omega$. Thus, the real and imaginary components of the permittivity are determined from α and n through

$$\varepsilon' = n^2 - k^2 \tag{4}$$

and

$$\varepsilon'' = 2\ n\ k. \tag{5}$$

Native conductivity arising from thermally excited conduction-band electrons was calculated from Eq. (3) by using the high temperature permittivity as $\hat{\eta}$ and the permittivity at 10 K as $\hat{\varepsilon}$. The real and imaginary parts of the conductivity are given by

$$\sigma' = \varepsilon_0 \omega(\eta'' - \varepsilon''), \tag{6}$$

$$\sigma'' = \varepsilon_0 \omega(\varepsilon' - \eta'). \tag{7}$$

This calculated conductivity is actually the change in conductivity compared to the 10 K reference, but since the conductivity at 10 K is negligibly small compared to that at high temperature, we treat them here as absolute conductivities.

The real and imaginary components of the complex conductivity for each temperature are shown in Figs. 2(a) and 2(b) as a function of frequency. We attribute all measured conductivity to electrons and not holes because the ZnO wafer is n type. All intrinsic ZnOs are n type, and donor densities are often an order of magnitude larger than acceptor densities.[8] Additionally, the effective mass of the electron in ZnO is about half that of the hole, so electron mobility will be larger and free-carrier THz absorption greater than that for holes.[29] Both real and imaginary conductivities increase with increasing temperature as more electrons are thermally excited into the conduction band. At 30 K and below, the free-carrier density is so low that the conductivity is not significantly different from that at 10 K. The real conductivities have their maximum at low frequency and decrease with increasing frequency. Imaginary conductivities are zero at low frequency, display a maximum at frequencies near 0.5 THz, and then decrease at high frequency.

The complex conductivity data at each temperature can be fit by the Drude model, which is the most common and straightforward model for conductivity in metals and semiconductors. The Drude model considers a free electron gas with complete momentum randomization following elastic scattering events, where the probability of a collision during a time interval dt is dt/τ where τ is the characteristic

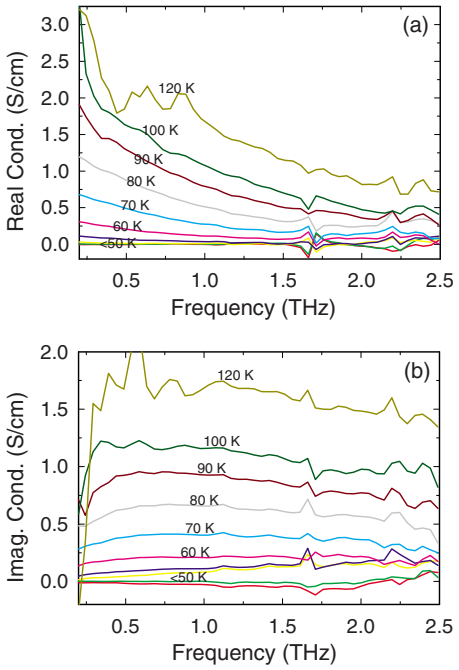

FIG. 2. (Color online) (a) Real and (b) imaginary conductivities of a ZnO wafer in the THz frequency range for temperatures ranging from 20 to 120 K. Conductivities are measured relative to the conductivity at 10 K.

scattering time. The frequency-dependent conductivity based on the Drude model is given by

$$\hat{\sigma}(\omega) = \frac{\varepsilon_0 \omega_p^2 \tau}{(1 - i\omega\tau)}, \tag{8}$$

where ε_0 is the permittivity of free space and ω_p is the plasma frequency.[30] The electron density, N_e, and plasma frequency are related through

$$N_e = \frac{\varepsilon_o \omega_p^2 m^*}{e^2}. \tag{9}$$

The dc mobility, μ, for a Drude conductor is given by

$$\mu = \frac{e\tau}{m^*}, \tag{10}$$

where e is the magnitude of the electron charge and m^* is the electron effective mass which is 0.24 m_e for ZnO.[29] The Drude model dictates that the real component of the conductivity has its maximum value at dc and that the imaginary component is positive with a maximum at the frequency of the carrier scattering rate.

For example, Figs. 3(a)–3(c) show the results of fitting the Drude model to the measured conductivity at 90, 70, and 50 K, respectively. The real and imaginary conductivities are fit simultaneously to determine ω_p and τ. The fit is reasonably good at high temperatures but becomes increasingly poor at low temperatures. However, even at high temperatures the best fit of the Drude model consistently overestimates the real conductivity at low frequencies while underestimating it

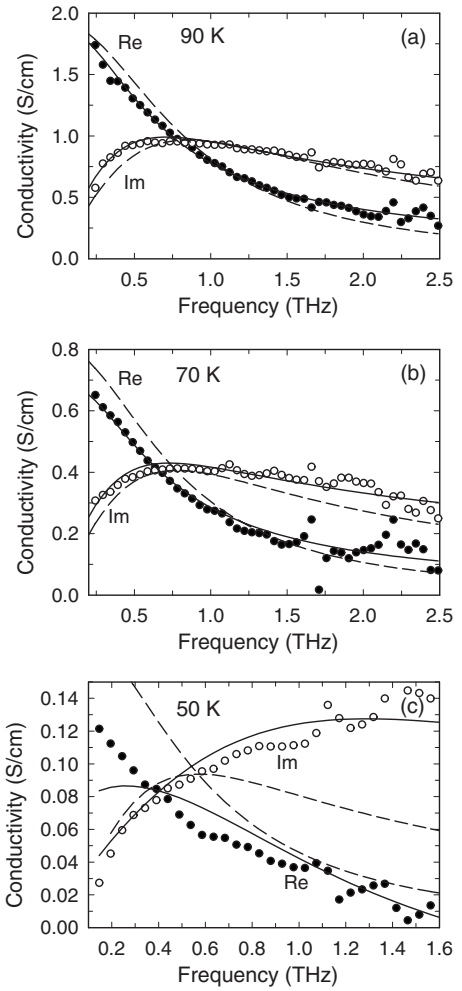

FIG. 3. Frequency-dependent real (solid circles) and imaginary (open circles) conductivity of the ZnO wafer with fits from Drude model (dashed lines) and the generalized Drude model (solid lines) for temperature of (a) 90, (b) 70, and (c) 50 K. At higher temperatures, small but systematic deviations of the Drude model are eliminated by use of the generalized Drude model. Significant hopping conduction is suspected at low temperature, and the fit with the generalized Drude is less satisfactory. Note the different scale in (c), in which data at 50 K were only fit below 1.6 THz due to noise at higher frequencies.

at high frequencies. Additionally, the peak for the imaginary conductivity is too sharp and underestimates the experimental values at both low and high frequencies.

While the Drude model fits the high-temperature data reasonably well to first order, the aforementioned deviations can be eliminated by refinement of the model. The Drude model assumes a single characteristic relaxation time. A distribution of relaxation times can be included by using the GD model, which incorporates both the Cole-Cole and Cole-Davidson modifications to the Drude model.[26] The GD model,

$$\hat{\sigma}(\omega) = \frac{\varepsilon_0 \omega_p^2 \tau}{(1 - (i\omega\tau)^{1-\alpha})^{\beta}}, \tag{11}$$

includes both symmetric and asymmetric logarithmic distributions of relaxation times. The Cole-Cole model incorporates only the symmetric distribution centered at $\ln \tau$ whose width increases with α, while the Cole-Davidson model incorporates a one-sided logarithmic distribution described by β. In the limits of $\alpha \to 0$ and $\beta \to 1$, the GD model reduces to the Drude model. Deviations from the Drude model in studies of THz permittivity have previously been treated using Cole-Cole, Cole-Davidson, or GD models for several other semiconductors including Si (Refs. 21 and 31) and GaAs.[26]

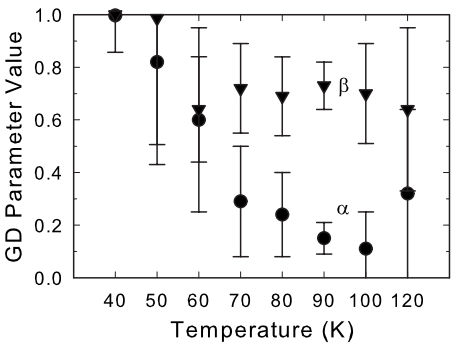

FIG. 4. α (circles) and β (triangles) parameters from fitting the Generalized Drude model to conductivity data as a function of temperature. $\beta \sim 0.7$ indicates fractal conductivity in the crystalline ZnO, independent of temperature in this range. α approaches zero for higher temperatures, approaching Drude-like behavior. Error bars are 90% confidence intervals.

The GD model provides an excellent fit to the experimental data for all temperatures above 50 K, eliminating the systematic deviations that existed with the Drude model. GD fits are shown along with Drude fits in Fig. 3. However, at temperatures of 50 K and below, the GD model cannot reproduce the imaginary conductivity, which continues to increase with increasing frequency. Additionally, the rate of increase in real conductivity with deceasing frequency near dc cannot be captured. These deviations are further exaggerated at 40 K (not shown). Conductivities at 20 and 30 K are very small, barely larger than the noise, and a unique set of best fit parameters cannot be determined. It is only possible to say that the electron densities are much smaller than 10^{13} cm^{-3}.

Values for the α and β parameters are plotted as a function of temperature in Fig. 4 to examine deviations from the Drude model. Error bars represent 90% confidence intervals on the fitted values of the GD model. α decreases with increasing temperature, from 0.60 at 60 K to 0.11 at 100 K, approaching the value of zero given by the Drude model. Although α increases slightly at 120 K, there is significant uncertainty in the fit at 120 K due to the low THz transmission at this temperature. β is approximately 0.7 for all temperatures above 50 K. Niklasson showed that a value of $\beta = 0.72$ arises from fractal conduction processes with a cutoff and is related to percolation theory.[32,33] Fractal conduction processes can result from either fractal structure, as in composites, or processes with fractal time dependence, such as multiple trapping. While band transport was expected rather than a hopping-type percolation, Jeon and Grischkowsky showed similar values of β for doped silicon with very low carrier densities below $\sim 10^{16}$ cm^{-3}.[21,31] As will be discussed shortly, carrier densities in this study were also below

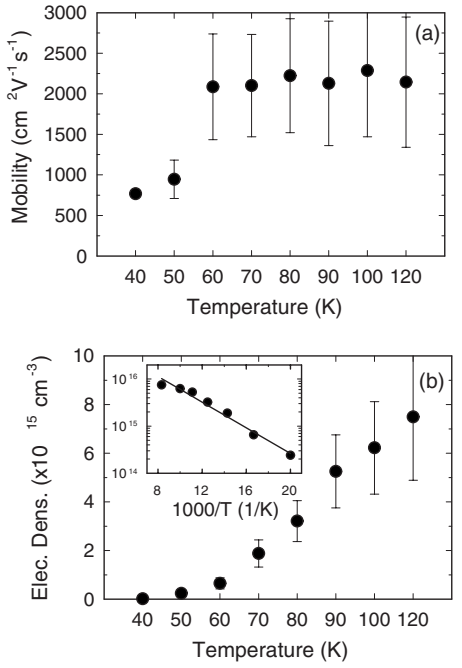

FIG. 5. Temperature-dependent (a) mobilities and (b) electron densities calculated by fitting the Generalized Drude model to experimental conductivity data. Error bars are 90% confidence intervals. Inset to (b) is an Arrhenius plot of electron density which shows an activation barrier of 27 meV.

$\sim 10^{16}$ cm^{-3}, and we conclude that fractal conduction is also possible in crystalline ZnO. We believe that fractal conduction results here because a portion of the electron transport occurs by hopping between localized traps whose spatial and energy distributions result in a fractal distribution of waiting times. The values of α and β both approach one at 40 and 50 K. While β of unity would simply reduce the GD model to the Cole-Cole model, α approaching unity indicates a fundamentally different mode of charge transport at low temperatures that does not satisfy the assumptions of the GD model.

Look suggested that conduction-band transport dominates above 40 K, with mixed band and hopping conductions for $15 < T < 40$ K, and primarily hopping transport that is limited by the acceptor concentration below 15 K.[8] The poor fit of the GD model to our experimental data and the significant change in the α and β parameters at temperatures below 50 K also indicate a transition in the mechanism of charge transport at low temperatures.

Electron density and mobility were determined by fitting the GD model to the complex conductivity data at each temperature and are shown in Fig. 5. The GD model shows mobilities of ~ 2100 cm^2 V^{-1} s^{-1} at 60 K and above, Fig. 5(a). Error bars represent 90% confidence intervals on the fitted values of the GD model. Within this degree of confidence, the mobility appears to be independent of or only weakly dependent on temperature in the 60–120 K range. Mobility decreases at lower temperature, which we attribute to a combination of increased ionized impurity scattering and a transition to hopping conduction.[8,34] We expect that mobility would also decrease at temperatures higher than 120 K due to increased lattice scattering, but conductivity could not be measured at higher temperatures because THz transmission was too small.

Magnitudes and trends of mobilities are fairly similar to those measured using the Hall effect by Look *et al.* for wafers grown by vapor transport.[8,17] Look measured Hall mobilities of 200 cm^2 V^{-1} s^{-1} at room temperature which increased to a maximum of 1900 cm^2 V^{-1} s^{-1} at 60 K and then decreased quickly to less than 500 cm^2 V^{-1} s^{-1} at 20 K. Hall mobilities differ from drift mobilities by the Hall r factor, which is typically in the range of 1.2–1.6 for ZnO.[17] With this correction, drift mobilities measured by THz-TDS are $\sim 50\%$ higher than those measured by Hall effect. Hall measurements also show mobilities which peak more sharply as a function of temperature. The difference between these techniques may result because THz-TDS samples electrons from the entire thickness of the wafer, while Hall experiments measure conductivity from a sheet of electrons near the surface.[35] Near-surface electrons can dominate the conductivity and obscure the determination of bulk properties. Additionally, the thickness of this sheet is not always well known, potentially leading to errors in measuring carrier concentration. Differences in mobilities between the two methods may also arise because the ac THz field oscillates carriers over distances of nanometers to microns, while Hall effect is a dc measurement which moves carriers over millimeters, allowing more carriers to interact with sparse defects.

Electron density rises exponentially with increasing temperature as electrons are thermally excited into the conduction band from shallow donor states [Fig. 5(b)]. Fits of the GD model to the conductivity data show electron density increasing from 1×10^{13} cm^{-3} at 40 K to almost 8×10^{15} cm^{-3} at 120 K. The temperature dependence of the electron densities determined by the GD fits are well described by an Arrhenius model, as shown in the inset in Fig. 5(b), with an activation energy of 27 meV. This shallow donor energy is consistent with the 25–35 meV range found for many different samples by Look *et al.*,[8,17] who showed that this donor is in fact a native defect that dominates the low-temperature electrical measurements. Specifically, their irradiation studies indicate that this defect is Zn_I. However, the possibility that the shallow donor is hydrogen related cannot be excluded.[10,36] No attempt was made to identify the nature of the donor in this work, only its activation energy. While measurements of conductivity could not be made above 120 K because of the strong THz absorption, we extrapolate from the Arrhenius fit that the room-temperature electron density is 5×10^{16} cm^{-3} and the donor density, found from the high-temperature intercept, is 1.4×10^{17} cm^{-3}.

IV. CONCLUSIONS

We have measured the conductivity of a ZnO wafer as a function of temperature using THz-TDS. Independent measurements of the power and phase allow calculation of absorption and refractive index, and hence complex permittivity, without the use of Kramers-Kronig relations. Mobilities measured by THz-TDS are in agreement with those measured by Hall effect, but THz-TDS provides additional rich information through the frequency-dependent complex con-

ductivity that is not accessible using dc electrical measurements. Specifically, we have found that conductivity at temperatures above 50 K behaves according to the Generalized Drude model with $\beta=0.7$, indicating fractal conductivity. Conversely, conductivity below 50 K indicates hopping transport. Temperature-dependent carrier concentration was fit to an Arrhenius model which shows a barrier of 27 meV for the native shallow donors.

ACKNOWLEDGMENTS

Acknowledgment is made to the Donors of the American Chemical Society Petroleum Research Fund for partial support of this research. C.A.S. acknowledges the National Science Foundation (Grant No. CHE-0616875) for partial support of this work.

*Corresponding author.
†jbaxter@drexel.edu
‡charles.schmuttenmaer@yale.edu

[1] U. Özgür, Y. I. Alivov, C. Liu, A. Teke, M. A. Reshchikov, S. Dogan, V. Avrutin, S. J. Cho, and H. Morkoc, J. Appl. Phys. **98**, 041301 (2005).
[2] D. C. Look, Mater. Sci. Eng., B **80**, 383 (2001).
[3] D. M. Bagnall, Y. F. Chen, Z. Zhu, T. Yao, S. Koyama, M. Y. Shen, and T. Goto, Appl. Phys. Lett. **70**, 2230 (1997).
[4] R. L. Hoffman, B. J. Norris, and J. F. Wager, Appl. Phys. Lett. **82**, 733 (2003).
[5] T. Minami, Semicond. Sci. Technol. **20**, S35 (2005).
[6] F. Hamdani *et al.*, Appl. Phys. Lett. **70**, 467 (1997).
[7] K. Maeda, M. Sato, I. Niikura, and T. Fukuda, Semicond. Sci. Technol. **20**, S49 (2005).
[8] D. C. Look, D. C. Reynolds, J. R. Sizelove, R. L. Jones, C. W. Litton, G. Cantwell, and W. C. Harsch, Solid State Commun. **105**, 399 (1998).
[9] J. Nause and B. Nemeth, Semicond. Sci. Technol. **20**, S45 (2005).
[10] C. G. Van de Walle, Phys. Rev. Lett. **85**, 1012 (2000).
[11] C. A. Wolden, T. M. Barnes, J. B. Baxter, and E. S. Aydil, J. Appl. Phys. **97**, 043522 (2005).
[12] M. D. McCluskey, S. J. Jokela, K. K. Zhuravlev, P. J. Simpson, and K. G. Lynn, Appl. Phys. Lett. **81**, 3807 (2002).
[13] E. V. Lavrov, J. Weber, F. Borrnert, C. G. Van de Walle, and R. Helbig, Phys. Rev. B **66**, 165205 (2002).
[14] X. N. Li, B. Keyes, S. Asher, S. B. Zhang, S. H. Wei, T. J. Coutts, S. Limpijumnong, and C. G. Van de Walle, Appl. Phys. Lett. **86**, 122107 (2005).
[15] Y. R. Ryu, S. Zhu, D. C. Look, J. M. Wrobel, H. M. Jeong, and H. W. White, J. Cryst. Growth **216**, 330 (2000).
[16] A. Tsukazaki *et al.*, Nature Mater. **4**, 42 (2005).
[17] D. C. Look, J. W. Hemsky, and J. R. Sizelove, Phys. Rev. Lett. **82**, 2552 (1999).
[18] J. B. Baxter and C. A. Schmuttenmaer, J. Phys. Chem. B **110**, 25229 (2006).
[19] D. L. Rode, *Semiconductors and Semimetals* (Academic Press, New York, 1975), Vol. 10, p. 1.
[20] J. B. Baxter and C. A. Schmuttenmaer, in *Terahertz Spectroscopy: Principles and Applications*, edited by S. L. Dexheimer (CRC Press, New York, 2008), p. 73.
[21] T. I. Jeon and D. Grischkowsky, Phys. Rev. Lett. **78**, 1106 (1997).
[22] M. van Exter and D. Grischkowsky, Phys. Rev. B **41**, 12140 (1990).
[23] T. I. Jeon, D. Grischkowsky, A. K. Mukherjee, and R. Menon, Appl. Phys. Lett. **77**, 2452 (2000).
[24] T. I. Jeon, K. J. Kim, A. K. Mukherjee, and R. Menon, Synth. Met. **150**, 53 (2005).
[25] G. H. Ma, D. Li, H. Ma, J. Shen, C. G. Wu, J. Ge, S. H. Hu, and N. Dai, Appl. Phys. Lett. **93**, 211101 (2008).
[26] M. C. Beard, G. M. Turner, and C. A. Schmuttenmaer, Phys. Rev. B **62**, 15764 (2000).
[27] P. U. Jepsen and B. M. Fischer, Opt. Lett. **30**, 29 (2005).
[28] A. K. Azad, J. G. Han, and W. L. Zhang, Appl. Phys. Lett. **88**, 021103 (2006).
[29] L. E. Brus, J. Chem. Phys. **80**, 4403 (1984).
[30] N. W. Ashcroft and N. D. Mermin, *Solid State Physics* (Thomson Learning, Inc., USA, 1976).
[31] T. I. Jeon and D. Grischkowsky, Appl. Phys. Lett. **72**, 2259 (1998).
[32] G. A. Niklasson, K. Brantervik, and L. Borjesson, J. Non-Cryst. Solids **131-133**, 1096 (1991).
[33] G. A. Niklasson, J. Appl. Phys. **62**, R1 (1987).
[34] X. C. Yang, C. C. Xu, and N. C. Giles, J. Appl. Phys. **104**, 073727 (2008).
[35] D. C. Look, Superlattices Microstruct. **42**, 284 (2007).
[36] Y. M. Strzhemechny *et al.*, Appl. Phys. Lett. **84**, 2545 (2004).